Journal of Applied Physics

Molecular dynamics study on Ar ion bombardment effects in amorphous SiO_2 deposition processes

Cite as: J. Appl. Phys. **100**, 123305 (2006); https://doi.org/10.1063/1.2401651
Submitted: 23 August 2006 . Accepted: 06 October 2006 . Published Online: 22 December 2006

Masafumi Taguchi, and Satoshi Hamaguchi

Molecular dynamics study on Ar ion bombardment effects in amorphous SiO_2 deposition processes

Masafumi Taguchi[a)]
Center for Atomic and Molecular Technologies, Graduate School of Engineering, Osaka University, 2-1 Yamadaoka, Suita, Osaka, 464-8603, Japan and Nippon Sheet Glass Co., 1 Kaidoshita, Konoike, Itami Hyogo 664-8520, Japan

Satoshi Hamaguchi[b)]
Center for Atomic and Molecular Technologies, Graduate School of Engineering, Osaka University, 2-1 Yamadaoka, Suita, Osaka 464-8603, Japan

(Received 23 August 2006; accepted 6 October 2006; published online 22 December 2006)

Argon ion bombardment effects on growing amorphous SiO_2 films during reactive sputtering deposition processes were examined based on molecular dynamics (MD) and Monte Carlo (MC) simulation techniques. The system we have considered here is a film that is subject to energetic Ar bombardment while it is formed by surface reactions of Si and O atoms separately supplied at low kinetic energies. It has been found that (1) Ar injections preferentially sputter O atoms from the surface over Si and (2) also have a compressing effect on the growing film during the deposition process. In other words, our MD/MC simulations have demonstrated at the atomic level that, with higher energy Ar injections, an amorphous SiO_2 film grown in a reactive sputtering deposition process is denser and more Si rich. © *2006 American Institute of Physics*.
[DOI: 10.1063/1.2401651]

I. INTRODUCTION

Reactive magnetron sputtering deposition processes have been used widely in the industry to produce various high-quality thin films. For example, they are known to be especially suitable for optical filter applications,[1–9] where high-yield formation of oxide thin films with complex stoichiometry (such as $TiNbO_x$) under strict control of film qualities is strongly required.

The density of a film made by a reactive magnetron sputtering process can be as high as that by an ion assisted deposition process. It is generally believed that this is due to bombardment of the film surface by ions that are produced by plasma in the chamber. However, details of the effects of ion bombardment during reactive magnetron sputtering deposition processes have not been well understood to date, at least, at the atomic level. For example, energetic ions incident to the surface may contribute to the increase of film density, but may also damage the film structures, depending on their energy. Chemical reactions that form new film layers with specific stoichiometry may also be strongly influenced by ion bombardment even if the energetic species are chemically inert. In addition, these effects may vary as the injection angles of all species.

The goal of the present study is to clarify such effects at the atomic level. We have developed numerical simulation techniques based on molecular dynamics (MD) and Monte Carlo (MC) simulations to emulate reactive deposition processes.[2,3] In our earlier studies[2,3] based on the numerical techniques, we examined characteristics of amorphous SiO_2 films deposited in reactive magnetron sputtering processes as functions of incident energy and angle for silicon and oxygen, without taking into account the effects of background argon or other species. However, in typical reactive magnetron sputtering systems that we are interested in for optical filter applications, Ar is widely used as a buffer gas to generate plasmas for magnetron sputtering and, due to the large Ar mass (larger than the Si mass), Ar bombardment is likely to have notable effects on the film formation. In the present work, therefore, we focus on argon bombardment effects on amorphous SiO_2 deposition.

A schematic diagram of the deposition system we consider here is given in Fig. 1. As in the reactive magnetron sputtering system considered in the previous studies of Refs. 1–3, Si atoms are sputtered from a Si target of the magnetron

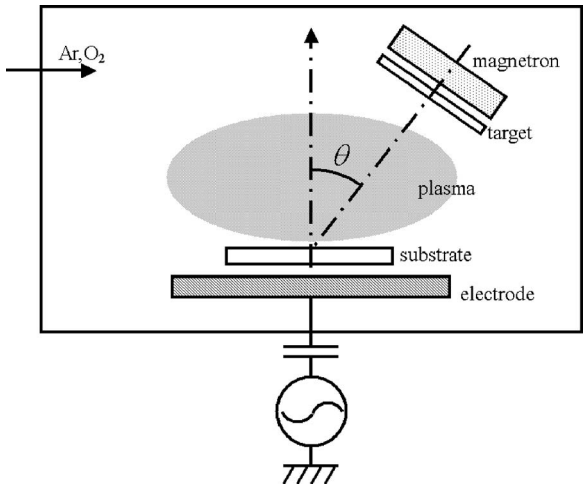

FIG. 1. A schematic diagram of a reactive magnetron sputtering system considered in the present work.

a)Electronic mail: masafumitaguchi@mail.nsg.co.jp
b)Author to whom correspondence should be addressed; electronic mail: hamaguch@ppl.eng.osaka-u.ac.jp

sputtering system. Argon and oxygen gases are provided separately, and the system is usually operated at low pressures, e.g., in the range of 0.1–3.0 Pa. These gases are used to generate plasma in front of the target to sputter Si atoms and also to decompose molecular oxygen into highly reactive O atoms. The sputtered Si atoms react with such O atoms (as well as O_2 molecules, possibly) to form SiO_2 near or on the substrate surface. The temperature of the substrate and gases are typically kept at 473 K. The Ar gas also acts as a diluent for the control of stoichiometry and other properties of deposited films. The Si sputtering target can be placed with an oblique angle θ from the normal direction of the substrate. In the present system, the substrate can be negatively biased by the rf electrode, which allows Ar ion bombardment with specific injection energies.[10–14]

The interatomic potential functions for Si and O used in our MD/MC simulations are of Stillinger-Weber type[15–18] and the same as those used in our previous work.[2,3] These classical interatomic potential functions are used to represent short-range interactions of covalent bonds. In our analyses, MD simulations are used to analyze the motion of atoms near or on the substrate surface for a relatively short period (e.g., duration of about 1 ps) around the moment of atomic impact. A slow thermal relaxation process that follows is emulated by MC simulations.[19] At the atomic level, a film deposition process consists of the repetition of atomic impact on the surface and thermal relaxation before the next atomic impact, so the MD/MC cycles are repeated during the simulation.

The rest of the paper is organized as follows. In the next section, we briefly discuss the simulation methods employed in the present work. In Sec. III, simulation results are presented together with discussion on possible mechanisms accounting for the observed phenomena. The summary is given in Sec. IV.

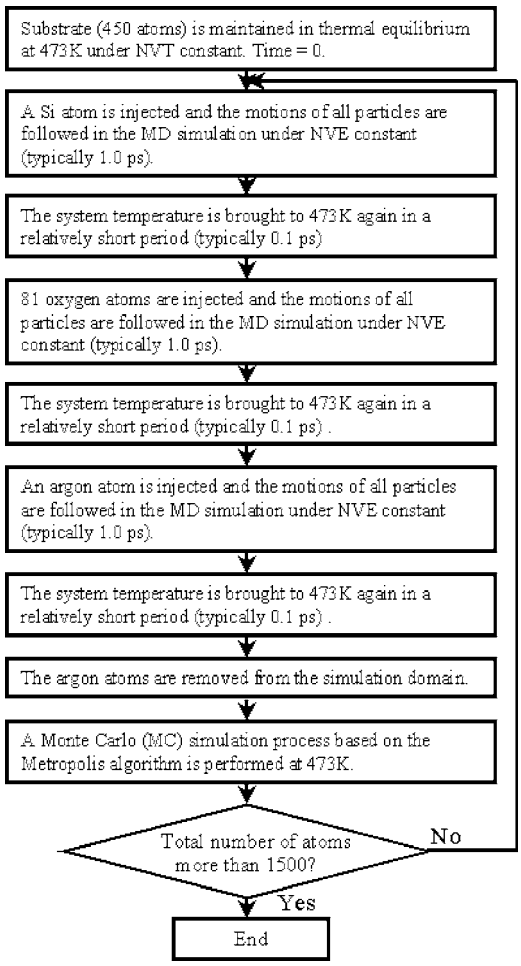

FIG. 2. A flow chart of the numerical procedure. Here "NVT constant" means simulation under the constant number of particles (N), volume (V), and temperature (T), i.e., of canonical ensemble. Similarly, "*NVE* constant" means simulation of microcanonical ensemble, where E stands for the total energy. The deposition simulation stops when 1500 atoms are accumulated in the simulation box.

II. SIMULATION METHODS

In this work, we simulate dynamics of sputtered Si atoms, a large number of low energy reactive O atoms, and energetic Ar ions that arrive at the surface of deposited film and form new layers of the film after some interactions, using MD/MC simulations. For the sake of simplicity, we assume that the flux of sputtered Si atoms is the same as that of Ar ions, which are much smaller than the flux of low energy O atoms. Assuming that oxygen molecules are mostly decomposed to O atoms in the plasma and surface reactions involving oxygen can be well represented by those of O atoms, we ignore the presence of O_2 molecules in the system in the simulations presented here.

The numerical procedures used in our simulations are summarized in the flow chart given in Fig. 2. The details of MD and MC methods may be found, for example, in Refs. 2, 3, 17, and 18. The simulation is carried out in a rectangular box, whose top and bottom surfaces are 2.4×2.4 nm^2 wide. The periodic boundary conditions are imposed in the horizontal directions of the simulation box. A crystalline SiO_2 that consists of 450 atoms and is 0.89 nm thick is placed at the bottom of the simulation box as the initial substrate and set to be in thermal equilibrium at 473 K. The positions of bottom atoms are fixed during simulation, which prevents the entire substrate from moving downward when it is subject to atomic bombardment. In a single deposition simulation, the cycle given in Fig. 2 was repeated until 1500 atoms were accumulated in the simulation box, including the 450 atoms of the initial substrate.

As described in Fig. 2, a single simulation cycle starts from the injection of a Si atom with 1 eV into the substrate surface from above. The horizontal position of an incident atom is randomly selected, and its vertical position is selected in such a way that it is high enough for the atom not to have interactions with other atoms on the substrate but close enough for it to reach the surface in a short time. The incident angle θ of Si is selected to be either 0 (i.e., normal injection) or 60° from the normal direction of the substrate. The motions of all atoms in the simulation box are then solved by the MD method under the condition of constant total energy (i.e., microcanonical simulation) for 1 ps. If there are any reflected or sputter atoms existing during this period, they are removed from the simulation box, and then

the temperature of the system is brought back to the initial substrate temperature in a relatively short period (typically 0.1 ps).

The next step is to bring a large number of O atoms (81 atoms in our simulations) almost simultaneously to this substrate with 0.8 eV, which models the flux of low energy charge neutral oxygen in the system. The angle of incidence for all O atoms is selected to be 0, i.e., normal injection for the sake of simplicity. The motions of all atoms are again solved in the MD method under microcanonical conditions for 1 ps. In this process, most of injected oxygen atoms are reflected. After all reflected and sputtered atoms are removed from the simulation box at the end of the microcanonical simulation, the substrate with some deposited atoms is again brought to thermal equilibrium at the initial substrate temperature.

The cycle up to this stage is the same as that used in our previous work.[2,3] Before proceeding to the discussion on the step of Ar injection, we comment on some assumptions made above.

Under the experimental conditions considered here, the kinetic energies of oxygen atoms are in the range of thermal energy at 473 K, which is significantly lower than 0.8 eV of oxygen injection energy selected for our simulations. The use of 0.8 eV, rather than the actual thermal energy, in the simulations is to avoid too slow gas-phase transport of oxygen atoms and thus to save simulation time. Effects of oxygen impact at 0.8 eV, rather than that at thermal energy, will be the subject of future study although we do not expect them to be significant, judging from our preliminary simulations with various oxygen injection energies less than 1 eV.

The magnitude of Si flux estimated from typical deposition rates observed in various experimental systems is about 16 $nm^{-2}\,s^{-1}$, which is much smaller than the typical oxygen flux (of the order of 6×10^3 $nm^{-2}\,s^{-1}$) under the experimental conditions mentioned above. The ratio of the oxygen flux to the flux of sputtered Si in the real system is much larger than the ratio of the number of injected O atoms, i.e., 81, that we employed per Si injection for the simulation. However, the number of O atom injection that we used here, i.e., 81, is nevertheless sufficiently large compared with the number of possible adsorption sites on the surface of simulation cell. Therefore, increasing it to a value higher than 81 would not affect the simulation results presented here.

The injection step for Ar in the simulation is similar to that for Si. After the step of oxygen injection was completed, a single Ar atom is injected to the substrate surface with a given kinetic energy (in the range of 10–100 eV) from above. Under typical experimental conditions (e.g., T_e = 10 eV, $n_i=1\times10^9$ cm^{-3} with T_e and n_i being the electron temperature and ion density), the magnitude of Ar ion flux estimated from the Bohm sheath criterion is about 5 $nm^{-2}\,s^{-1}$, which is close to the Si flux mentioned above. In our simulations, an Ar ion is injected per Si injection for simplicity. After Ar injection, the motions of all particles are again simulated by the MD method under microcanonical conditions for 1 ps. When the injection energy is high, the injected Ar atom and/or substrate atoms scattered by it may pass though the bottom of simulation substrate. At the end of this simulation, reflected and sputtered atoms, as well as those that have passed though the bottom of the simulation substrate, are removed from the simulation box. The system temperature is then again lowered to the initial temperature. If any Ar atoms are still trapped in the substrate, which cannot form bonds with other atoms (due to their repulsive interactions with other atoms, as will be discussed shortly) and thus are expected to be desorbed from the surface eventually, they are also removed from the simulation box. Under typical simulation conditions, however, the number of Ar atoms accumulated in the simulation box is extremely small even without the Ar removal step mentioned above. Therefore effects of Ar accumulation are generally ignored.

After Ar injection, the MC simulation step is then carried out for all atoms in the system, which is to emulate thermal relaxation processes of the system. As discussed in Refs. 2 and 3, MC simulation is performed in the following manner. First we move a single atom of the system in the simulation cell by a small distance in an arbitrary direction and measure the change of the total potential energy. We adopt or do not adopt this atomic displacement based on the usual Metropolis algorithm.[19] We perform the same processes for all atoms in the system (except for the fixed atoms at the bottom of simulation box). We call this process of displacing all atoms, whether each displacement is adopted or not as the result of the Metropolis algorithm, one MC cycle. We typically use more than 800 MC cycles in a single step of MC simulation prior to the next injection of Si atom.

After the MC simulation step, if a sufficiently large number of atoms have been accumulated in the simulation box, we stop the simulation, as stated before. Otherwise, we repeat the process above, as indicated in Fig. 2.

As mentioned in the preceding section, the interatomic potential functions for Si and O used in the simulations are the same as those used in the previous work[2,3,17,18] and were originally developed by Watanabe *et al.* in Ref. 16. It is also assumed for the sake of simplicity that an ion has the same short-range interatomic potential functions as the corresponding charge neutral atom of the same kind. In other words, in our simulations, an ion and the corresponding charge neutral atom have the same chemical properties. In addition, as in earlier studies of Refs. 2, 3, 17, and 18, the potential functions used here assume a repulsive interaction between two O atoms, and, therefore, the formation of O_2 molecules or formation of a single bond between two O atoms (i.e.,–O–O–) are not considered in our simulations. Implementation of more elaborate potential functions among O atoms is deferred to a future study.

As to interaction potentials of Ar with Si and O, we have constructed new potential functions by fitting Stillinger-Weber-type functions to data obtained from *ab initio* potential calculations. Since the interaction is essentially two-body repulsive, the total potential energy of the Ar–Si (or Ar–O) system may be given by

$$\Phi = \sum_i \sum_{j>i} \varepsilon f_2(i,j), \tag{1}$$

where ε(=2.1695 eV) is the energy unit used in the Stillinger-Weber (SW) potential and

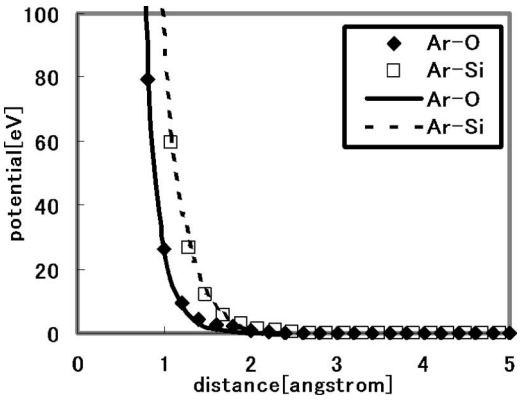

FIG. 3. Interatomic potential energies obtained from *ab initio* calculations for Ar–O (filled diamond) and Ar–Si (open square) pairs, together with the corresponding fitting functions given by Eq. (2) and Table I.

$$f_2(i,j) = A_{ij}(B_{ij}r_{ij}^{-p_{ij}} - r_{ij}^{-q_{ij}})\exp\frac{1}{r_{ij} - a_{ij}}, \tag{2}$$

if $r_{ij} < a_{ij}$, and $f_2(i,j) = 0$ otherwise. Here r_{ij} is the distance between atom i and atom j normalized by the unit length $\sigma = 2.0951$ Å and a_{ij} is the cutoff distance. Interatomic potential energies were obtained from *ab initio* calculations based on density functional theory (B3LYP) with the 6-311++G(d,p) basis set for Ar–Si and Ar–O pairs and are plotted in Fig. 3, where the fitting functions of Eq. (2) are also given by solid and broken curves. Parameter fitting was based on the Levenberg-Marquardt nonlinear fitting[21] and the obtained parameter values are given in Table I.

The interaction potentials of Ar with Si and O are also given in Ref. 17, which were derived from the widely used Molière potential.[20] The Si–Ar and O–Ar potential functions used in this work are essentially similar to those given in Ref. 17.

III. SIMULATION RESULTS AND DISCUSSION

Figure 4 shows typical atomic-scale morphologies of deposited SiO_2 film surfaces obtained from MD/MC simulations. The gray large sphere represents a Si atom and the light small sphere an O atom. As mentioned earlier, no Ar atom remains in the deposited film. In Fig. 4(a), no Ar was injected. In Figs. 4(b) and 4(c), Ar atoms were injected to the surface during the deposition processes with 35 and 100 eV. The angle of incidence for injected Si, O, and Ar atoms was selected to be 0, i.e., normal to the initial substrate surface. The film temperature was set at 473 K during the deposition processes. It is seen in Fig. 4 that the film becomes more densely packed as the Ar injection energy increases. By observing the motion of atoms obtained from simulations, we have confirmed that, at high injection energy, most Ar atoms make multiple collisions with Si and O atoms near the film surface and press them downwards in general. After making such collisions, the majority of injected Ar atoms are recoiled or reflected and leave the film surface in the upward direction. From the momentum conservation, therefore, the Ar collisions exert a downward average force to the deposited film, which is likely to make the film denser.

TABLE I. Numerical values for the fitting parameters of a Stillinger-Weber-type function given in Eq. (2) for Ar–O and Ar–Si pairs.

A_{ArO}	6.684	A_{ArSi}	6.721
B_{ArO}	1.176	B_{ArSi}	2.809
p_{ArO}	4.894	p_{ArSi}	3.376
q_{ArO}	4.895	q_{ArSi}	3.381
a_{ArO}	1.25	a_{ArSi}	1.25

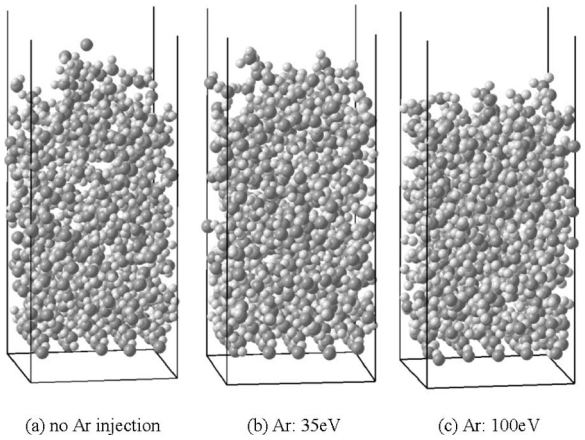

FIG. 4. Atomic-scale surface morphologies of deposited SiO_2 films obtained from MD/MC simulations. The gray large sphere represents a Si atom, and the light small sphere an O atom. The angle of incidence for all atoms is 0, i.e., normal to the initial substrate surface. The Si and O incident kinetic energies are 1 and 0.8 eV. In (a), no Ar is injected. In (b) and (c), the Ar incident energies are 35 and 100 eV. The film temperature is set at 473 K.

Figure 5 shows the radial distribution functions of a

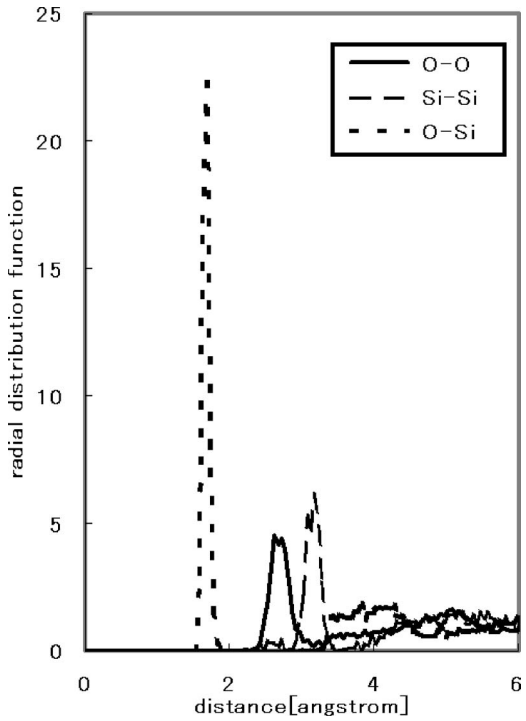

FIG. 5. The radial distribution functions of O–O (solid curve), Si–Si (broken curve), and O–Si (dotted curve) for a deposited film obtained from MD/MC simulations. The Si, O, and Ar incident energies are 1, 0.8, and 50 eV, respectively. The angle of incidence for all atoms is 0, i.e., normal to the initial substrate surface. The surface temperature is set at 473 K. The radial distribution functions shown here indicate that the film is amorphous.

SiO_2 deposited film obtained from MD/MC simulations. The deposition conditions are the same as those in Fig. 4, except that the Ar injection energy is 50 eV in this case. Here the radial distribution functions are evaluated only from the atoms located in the middle portion of the deposited film so that surface atoms should not affect the radial distribution functions. The radial distribution functions shown here are those of typical amorphous SiO_2.

Since Ar injections tend to damage the deposited film surface and create more surface dangling bonds, we expect that abundant neutral oxygen are likely to attach during the process. In other words, Ar injections may increase the sticking tendency of O atoms. However, Ar injections are also known to sputter surface oxygen;[18,22] the net effect of Ar injection on oxygen adsorption may not be straightforward. To clarify this effect, we first attempt to extract information on the tendency of Si or O to stick to a rough surface created by Ar bombardment. To this end we evaluate the "sticking number per Si injection" for a given species (i.e., Si or O), which we define as the number of atoms that stick to the surface at least tentatively before Ar sputtering, if any, may remove some of those atoms from the surface during the deposition process. More specifically, in the MD/MC simulations, in each cycle defined in Fig. 2, we count the number of Si (or O) atoms that newly stick to the surface during the cycle *before* the Ar injection step starts. The average of such numbers gives by definition the sticking number per Si injection for the species. Note that this number for Si is nothing but its sticking probability. However, for O atoms, whose possibility of sticking to the surface is limited by the number of Si dangling bonds available on the surface, the "sticking number of O per Si injection" is more directly related to the macroscopically observable adsorbed flux of oxygen, as will be discussed more in detail later.

Figure 6 presents the sticking numbers per Si injection defined above for Si (broken lines) and O (solid lines) as functions of Si dose, i.e., the accumulated number of Si atoms that arrive at (but not necessarily stick to) the unit surface area. In (a), no Ar is injected and, in (b), Ar atoms are injected with 50 eV. Other deposition conditions are the same as those in Figs. 4 and 5. The value at a given Si dose here is the average of the sticking number over 17 injection cycles of Fig. 2 (i.e., the average over the dose of 3.0×10^{14} cm^{-2}) around the specific injection cycle.

Some of Si and O atoms counted in Fig. 6(b) are removed from the surface by Ar sputtering. The sputtering yields (i.e., the numbers of atoms removed from the surface per Ar injection) for Si (broken curve) and O (solid curve) by 50 eV Ar injections during the deposition processes are plotted as functions of Ar dose in Fig. 7. The Ar dose used here is the same as the Si dose in Fig. 6 as we have assumed the equal fluxes for Si and Ar in our simulations, as described in the flow chart of Fig. 2. Other deposition conditions are also the same as those of Fig. 6(b). The yields here are evaluated from the numbers of Si and O atoms removed from the surface right after the Ar injection step in the flow chart of Fig. 2. As in Fig. 6, the value plotted at a specific Ar dose is the yield averaged over 17 injection cycles (i.e., over the dose of 3.0×10^{14} cm^{-2}) around the specific injection cycle. It is seen

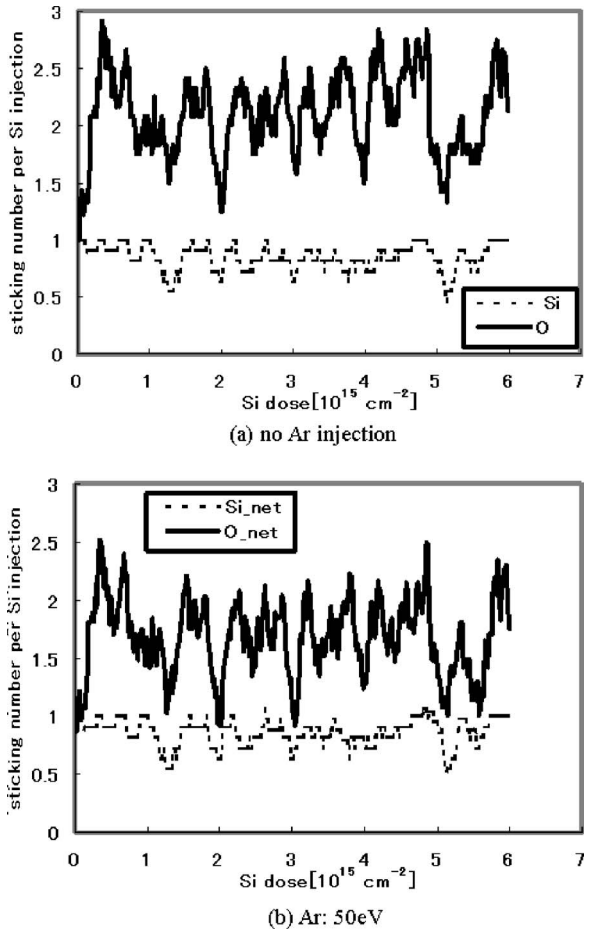

FIG. 6. The sticking numbers of Si (broken lines) and O (solid lines) per Si injection, i.e., numbers of Si and O atoms that stick to the surface per Si injection before Ar sputtering, if any, may remove some of them from the surface during the deposition processes, are plotted as functions of Si dose. In (a), no Ar is injected and, in (b), the Ar injection energy is 50 eV. Other deposition conditions are the same as those in Figs. 4 and 5.

that the nature of surface changed at around the Ar dose of 3×10^{15} cm^{-2}, and the system indeed is found to have reached steady state after this dose. By averaging the values given in Figs. 6 and 7 during the steady state, i.e., over

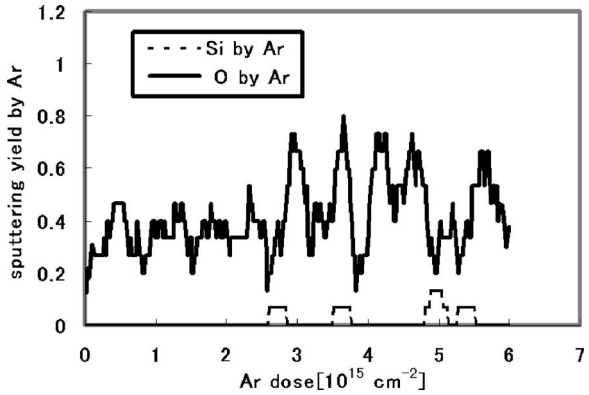

FIG. 7. Sputtering yields of Si (broken curve) and O (solid curve) by 50 eV Ar bombardment during the deposition process, the conditions of which are the same as those in Fig. 5. The horizontal axis represents Ar dose, which is the same as Si dose since the Si and Ar fluxes are assumed to be equal in our simulations. It is seen that the system reaches steady state after Ar dose reaches approximately 3×10^{15} cm^{-2}.

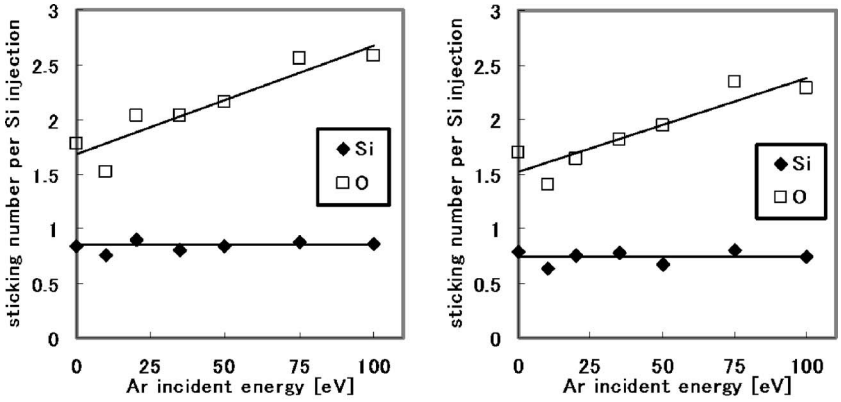

FIG. 8. The sticking numbers of Si (filled diamonds) and O (empty squares) per Si injection, i.e., the average numbers of Si and O atoms that stick to the surface per Si injection before Ar sputtering, if any, may remove some of them from the surface during the deposition processes. The value for Si is equivalent to its sticking probability. The horizontal axis represents the Ar incident energy. In (a) and (b), the angles of incidence for Si atoms are 0 and 60°. Other deposition conditions are the same as those of Figs. 4–7. The solid lines are merely guides to the eye.

sufficiently large Si or Ar dose after 3×10^{15} cm^{-2}, we obtain the (average) sticking numbers and sputtering yields of Si and O.

The sticking numbers obtained in this manner are given in Fig. 8 as functions of the Ar injection energy. The angles of incidence for O and Ar are both 0, i.e., normal to the initial surface. In (a) and (b), the angles of incidence for Si are 0 and 60°. In the deposition system depicted in Fig. 1, the angle of Si injection can be controlled by the position of its target, but the incident angle Ar ions is in general normal to the electrode since Ar ions are accelerated by the plasma sheath above it. The horizontal axis in Fig. 8 represents the Ar incident energy, and null energy is equivalent to no Ar injection since Ar has only a repulsive interaction with Si and O. The surface temperature is set at 473 K during the process. The solid lines are merely guides to the eye.

It is seen in Fig. 8 that the sticking number of Si, i.e., the sticking probability of Si, during the deposition process hardly depends on the Ar incident energy in both cases. This may be understood since an injected Si atom can stick to any dangling bonds of Si or O atoms on the surface, and therefore morphological changes of the surface caused by Ar sputtering hardly affect its ability to stick to the surface. On the other hand, as mentioned earlier, O atoms are allowed to form bonds only with Si atoms under the interatomic potential functions we employed here. Therefore, in addition to the dangling bonds of a newly deposited Si atom on the surface, Ar sputtering of surface O atoms can increase a chance for newly arrived O atoms to stick to the surface. This is likely to be the reason for the increase of the sticking number of O per Si injection as a function of the Ar incident energy.

As we showed in our previous work of Ref. 3, films formed by oblique Si injections have lower densities, more pores, and rougher surfaces. In other words, vertically injected Si atoms in Fig. 8(a) are likely to stick to the surface more firmly than obliquely injected Si atoms in Fig. 8(b). This seems to account for the slightly larger sticking number of Si in Fig. 8(a). Furthermore, as will be shown in Fig. 9, less firmly stuck Si atoms are more easily removed by Ar sputtering. Therefore, at a given Ar incident energy, the number of Si remaining on the surface is larger in the case of Fig. 8(a), which increases the number of dangling bonds to which O atoms can stick. This may be the reason that the sticking numbers of O are slightly larger in Fig. 8(a) than those in Fig. 8(b).

The sputtering yields of Si and O by Ar bombardment during the deposition processes are given as functions of Ar energy in Fig. 9. The deposition conditions in (a) and (b) are the same as those of Figs. 8(a) and 8(b). The solid lines, which are given by $y=0.045(x-10)^{0.66}$ for (a) and $y=0.054(x-10)^{0.66}$ for (b), with x and y being the energy in eV and sputtering yield, are merely guides to the eye. It is seen that Si sputtering yields are extremely small, whereas O sputtering yields increase significantly with the Ar incident energy. The threshold for O sputtering is about 10 eV in both

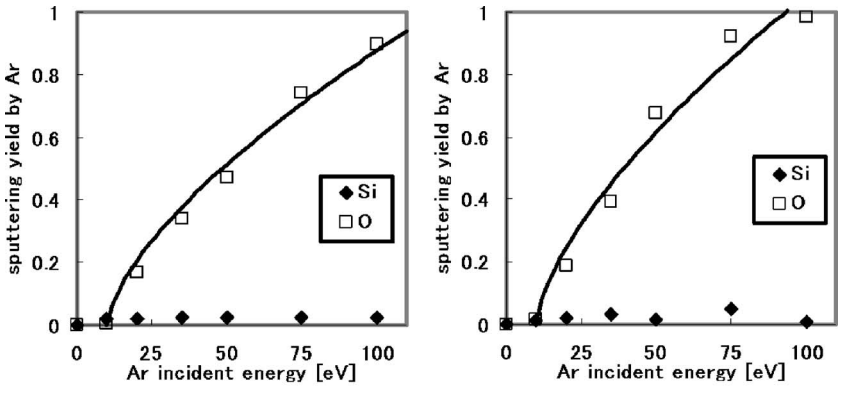

FIG. 9. Sputtering yields of Si (filled diamonds) and O (empty squares) by Ar bombardment during the deposition processes as functions of Ar incident energy. The deposition conditions in (a) and (b) are the same as those of Figs. 8(a) and 8(b). The solid lines are merely guides to the eye. In both cases the Si sputtering yields are extremely small, whereas the O sputtering yields are strong increasing functions of the Ar incident energy with the threshold value of about 10 eV.

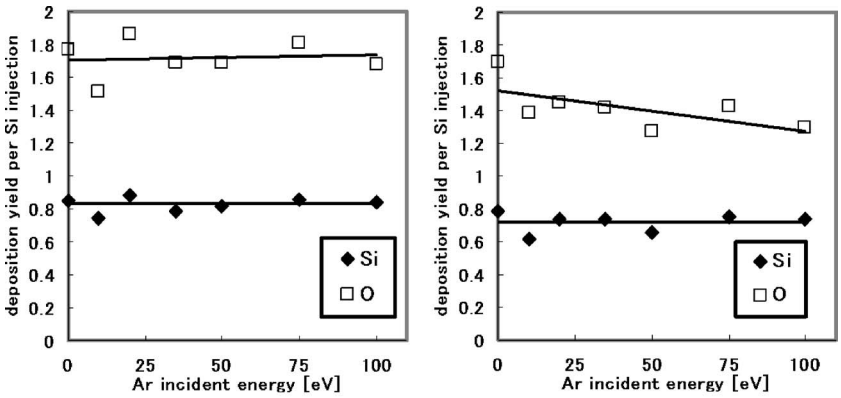

FIG. 10. Deposition yields per Si injection for Si (filled diamonds) and O (empty squares), i.e., the numbers of deposited atoms per Si injection during the deposition processes as functions of the Ar injection energy. The deposition conditions in (a) and (b) are the same as those of Figs. 8(a) and 8(b). The solid lines are guides to the eye. It is seen in both cases that, for a given incoming Si flux, the adsorbed Si flux during the deposition process (i.e., Si deposition rate) is almost independent of the Ar incident energy, whereas the adsorbed O flux (i.e., O deposition rate) is a weakly decreasing function of it. In other words, Ar injections may be considered to preferentially sputter O atoms from the surface.

cases shown here. Since O atoms are continuously supplied and cover the film surface, large sputtering yields for O obtained here are not unexpected.

It is also seen that the sputtering yields for Si and O in Fig. 9(a) are somewhat smaller than those in Fig. 9(b). This is likely to be caused by the nature of a deposited film formed by oblique Si injections, which is less dense and more porous, as mentioned before. Therefore, for such films used in Fig. 9(b), more loosely adsorbed Si and O atoms on rougher surfaces are more easily sputtered by incident Ar atoms.

If we measure the "deposition rate" for specific atomic species (Si or O) by the number of atoms deposited per unit area per unit time in the deposition process (rather than the usual definition as the thickness of film deposited per unit time), the deposition rate of Si or O (which is equivalent to the adsorbed flux of Si or O) normalized by the Si incoming flux is the value obtained as the difference between the sticking number and the sputtering yield given in Figs. 8 and 9. We call this value the "deposition yield per Si injection" and plot the values for Si and O in Fig. 10. It is shown in both cases that, for a given incoming Si flux, the adsorbed Si flux during the deposition process (i.e., Si deposition rate) is almost independent of the Ar incident energy, whereas the adsorbed O flux (i.e., O deposition rate) is a weakly decreasing function of the Ar incident energy.

Figure 11 shows the film densities as functions of the Ar incident energy. The deposition conditions for Figs. 11(a) and 11(b) are the same as those in Figs. 8(a) and 8(b). The film density is evaluated only from the atoms located in the middle portion of the deposited film, so that the density given in Fig. 11 is more representative of the bulk density, rather than the density of the very top surface layers of the film. It is clearly seen that the momentum transfer from Ar ions compresses the film and makes it denser in both cases of (a) and (b). The compressing effect by Ar bombardment is more pronounced in the case of a less dense film given in Fig. 11(b).

Figure 12 shows the stoichiometries of deposited films as functions of the Ar incident energy. The stoichiometry is defined as the ratio of the number of O atoms to that of Si atoms in the bulk of the deposited film. For crystalline SiO_2, this ratio, which we here denote by O/Si, is 2. The deposition conditions for (a) and (b) are the same as those in Figs. 8(a) and 8(b). For Fig. 12, the stoichiometry was evaluated only from the atoms located in the middle portion of the deposited film, as in Fig. 11. The film is shown to become more Si rich as the Ar incident energy increases in both cases of (a) and (b). In other words, Ar injections preferentially sputter O atoms from the surface. As shown in Ref. 3, the film in Fig. 12(b) is more oxygen rich without Ar injections. The oxygen reduction effect by Ar sputtering seems to be more pronounced in the initially more oxygen rich and less dense film of Fig. 12(b).

Figure 13 shows the coordination numbers of Si for O in the bulk of deposited films as functions of the Ar incident

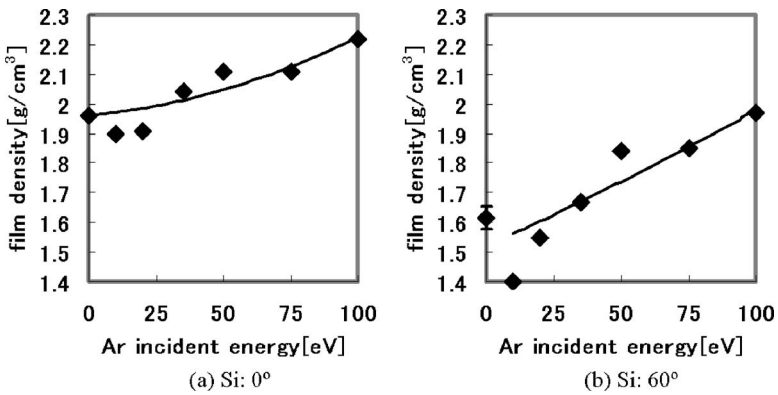

FIG. 11. The film densities as functions of the Ar incident. The deposition conditions for (a) and (b) are the same as those in Figs. 8(a) and 8(b). The film density is shown to increase as the Ar incident energy increases. The solid lines are guides to the eye.

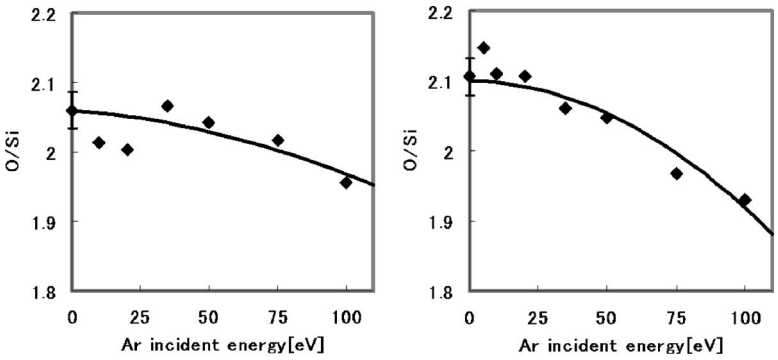

FIG. 12. The stoichiometries of deposited films as functions of the Ar incident energy. The stoichiometry is defined as the ratio of the number of O atoms to that of Si atoms (which is denoted by O/Si) in the bulk of deposited film. The deposition conditions for (a) and (b) are the same as those in Figs. 8(a) and 8(b). The film is shown to become more Si rich as the Ar incident energy increases. In other words, Ar injections may be considered to preferentially sputter O atoms from the surface. The solid lines are guides to the eye.

energy. The deposition conditions for (a) and (b) are the same as those in Figs. 8(a) and 8(b). The coordination number of Si for O is defined as the number of bonds of a Si atom connected with O atoms. For crystalline SiO_2, the coordination number of Si for O is 4. As in Figs. 11 and 12, we evaluated the coordination number only from the atoms located in the middle portion of the deposited film in order to avoid counting those of surface atoms, which tend to have more dangling bonds and/or oxygen terminated bonds. The coordination number is shown to decrease as the Ar incident energy increases in both cases. This is consistent with the observation in Fig. 12 that the film becomes more Si rich as the Ar incident energy increases.

In Figs 12 and 13, we examined how the local arrangement of Si and O atoms changes under the influence of Ar bombardment. Such local (i.e., short-scale) arrangements of neighboring Si and O atoms are called the short-range order (SRO). In the process of densification, however, it has been suggested[23] that the medium range order (MRO) of the film, rather than the short-range order (SRO), undergoes an even more significant change as a result of the change in arrangement of the $Si(O_{1/2})_4$ tetrahedra in the film. Although a detailed analysis of the MRO of the films presented here is outside the scope of the present work, it may elucidate the mechanism of film densification by energetic bombardment.

IV. SUMMARY

We have examined Ar ion bombardment effects during reactive sputtering deposition processes for the growth of amorphous SiO_2 films. The formation of SiO_2 essentially takes place on the film surface when Si atoms supplied from a magnetron sputtering target that is set away from the substrate react with a separately supplied (low-pressure) oxygen gas. Since plasma exists in the reaction vacuum chamber, we assume that some oxygen molecules are broken into highly reactive O atoms and therefore have focused on surface reactions of silicon and atomic oxygen. Assuming a simple model where a single Si atom and many O atoms are injected to the surface alternatively at 1 and 0.8 eV with given angles of incidence, we have analyzed dynamics of such atoms using MD/MC simulations. In our previous studies,[2,3] we have evaluated some characteristics of deposited films under various deposition conditions for the same process without Ar sputtering.

In the deposition processes, an Ar gas that is used as a buffer gas and also as a diluent provides Ar ions that bombard the surface of the growing film. Without an externally applied bias voltage, the Ar bombardment energy is essentially determined by the plasma potential. The Ar injection energy can be further increased by the bias voltage applied to the substrate. Assuming that the Ar flux is equal to the Si flux, we simulated the growth process of amorphous SiO_2 films with Ar bombardment in the present study.

It has been found from the simulations that Ar bombardment, especially when its energy is sufficiently high, has essentially the following two distinct effects. One is that Ar injections preferentially sputter O atoms from the surface over Si, so that the film becomes more Si rich as Ar injection energy increases. The other is that Ar injections have a compressing effect on the growing film due to the momentum transfer. The combination of these two effects causes the increase of film density, Si content (i.e., the inverse of O/Si defined in the preceding section), and decrease of the coordination number of Si for O for the deposited film as the Ar

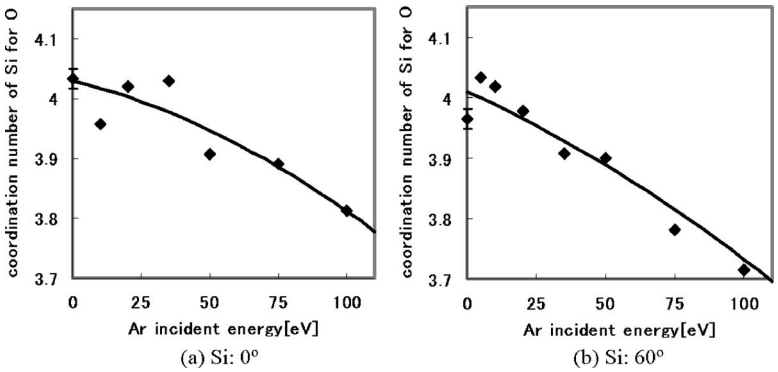

FIG. 13. The coordination numbers of Si for O in the bulk of deposited films as functions of the Ar incident energy. The coordination number of Si for O is defined as the number of bonds of a Si atom connected with O atoms. The deposition conditions for (a) and (b) are the same as those in Figs. 8(a) and 8(b). The coordination number is shown to decrease as the Ar incident energy increases. This is consistent with the observation in Fig. 12 that the film becomes more Si rich as the Ar incident energy increases. The solid lines are guides to the eye.

injection energy increases. Some preliminary examinations of film qualities obtained under various conditions in optical filter deposition processes[1] seem to indirectly support the two effects by Ar bombardment mentioned above. A qualitative comparison of the simulation results with experimental data is left for a future study.

[1]M. Taguchi, T. Kunisada, S. Kusaka, and S. Hamaguchi, IEEE Trans. Plasma Sci. **34**, 1084 (2006).
[2]M. Taguchi and S. Hamaguchi, Thin Solid Films (in press).
[3]M. Taguchi and S. Hamaguchi, Jpn. J. Appl. Phys., Part 1 **45**, 8163 (2006).
[4]J. Song, N. Zhu, and S. He, Opt. Commun. **252**, 247 (2005).
[5]W. Kong, Z. Shen, J. Shen, J. Shao, and Z. Fan, Optik (Jena) **116**, 325 (2005).
[6]P. I. Hagouel, Microelectron. Reliab. **43**, 249 (2003).
[7]Y. Hirai, K. Kanakugi, T. Yamaguchi, K. Yao, S. Kitagawa, and Y. Tanaka, Microelectron. Eng. **67–68**, 237 (2003).
[8]K. Shimmo *et al.*, Proceedings of National Fiber Optic Engineers Conference, 2001 (unpublished), Vol. 2, pp. 1101–1107.
[9]K. Nakama *et al.*, Proceedings of European Conference on Optical Communication 2001 (unpublished), Vol. 3, p. 426.
[10]S. M. Rossnagel and J. Hopwood, Appl. Phys. Lett. **63**, 3285 (1993).
[11]S. M. Rossnagel and J. Hopwood, J. Vac. Sci. Technol. B **12**, 449 (1994).
[12]S. Hamaguchi and S. M. Rossnagel, J. Vac. Sci. Technol. B **13**, 183 (1995).
[13]S. Hamaguchi and S. M. Rossnagel, J. Vac. Sci. Technol. B **14**, 2603 (1996).
[14]S. Hamaguchi, A. A. Mayo, S. M. Rossnagel, D. E. Kotecki, K. R. Milkove, C. Wang, and C. E. Farrell, Jpn. J. Appl. Phys., Part 1 **36**, 4762 (1997).
[15]F. H. Stillinger and T. A. Weber, Phys. Rev. B **31**, 5262 (1985).
[16]T. Watanabe, H. Fujiwara, H. Noguchi, T. Hoshino, and I. Ohdomari, Jpn. J. Appl. Phys., Part 2 **38**, L366 (1999).
[17]H. Ohta and S. Hamaguchi, J. Chem. Phys. **115**, 6679 (2001).
[18]H. Ohta and S. Hamaguchi, J. Vac. Sci. Technol. A **19**, 2373 (2001).
[19]N. Metropolis, A. W. Rosenbluth, M. N. Rosenbluth, A. H. Teller, and E. Teller, J. Chem. Phys. **21**, 1087 (1953).
[20]I. Torrens, *Interatomic Potentials* (Academic, New York, 1972).
[21]W. H. Press, S. A. Teukolsky, W. T. Vetterling, and B. P. Flannery, *Numerical Recipes in C*, (Cambridge University Press, Cambridge, England 1988).
[22]A. Kubota and D. J. Economou, IEEE Trans. Plasma Sci. **27**, 1416 (1999).
[23]A. Lefevre, L. J. Lewis, L. Martinu, and M. R. Wertheimer, Phys. Rev. B **64**, 115429 (2001).